Bulg. J. Phys. **46** (2019) 134–150

Analyzing Powers in Elastic e-d Scattering and Their Sensitivity to Nucleon Form Factors

E.M. Mahrous[1], **E.M. Darwish**[1,2], **H.M. Abou-Elsebaa**[1,2], **A. Hemmdan**[3],
[1]Physics Department, Faculty of Science, Taibah University, Saudi Arabia
[2]Physics Department, Faculty of Science, Sohag University, Egypt
[3]Physics Department, Faculty of Science, Aswan University, Egypt

Received: *18 March 2019*

Abstract. Influence of nucleon structure on single tensor-deuteron and double beam-vector-deuteron analyzing powers in the elastic electron-deuteron scattering process is investigated. We report numerical results for the tensor-deuteron (T_{20}, T_{21}, and T_{22}), and beam-vector-deuteron (T_{10} and T_{11}) analyzing powers as functions of the four-momentum transfer square Q^2 and the electron scattering angle in the laboratory frame θ_e. This is made possible with the advent of recent polarization measurements with polarized electron beams and/or polarized deuteron targets at MIT-Bates, JLab, NIKHEF, VEPP-2, and VEPP-3. We found that the predicted results for T_{21}, T_{22}, T_{10}, and T_{11} are sensitive to the nucleon electromagnetic form factors. On the contrary, the T_{20} analyzing power is found to be almost independent on the actual nucleon form factors. The predicted analyzing powers are compared with the available experimental data and a satisfactory agreement is obtained.

PACS codes: 25.30.Bf, 25.45.De, 13.40.Gp, 13.75.Cs, 14.20.-c

1 Introduction

Elastic electron-deuteron (e-d) scattering provides a very powerful tool to investigate the structure of the two-nucleon system and its electromagnetic properties. This reaction gives a direct way to study the properties of NN interaction and electromagnetic characteristics of nucleons. The elastic e-d scattering process has been studied for many years in the past, both theoretically and experimentally (see, for example, Refs. [1–12] and references therein). Notwithstanding, this reaction is still an extremely interesting and fascinating subject, and there is great need for much more detailed investigations.

The deuteron can be used to a good approximation as an effective neutron target for the measurements of the neutron electromagnetic form factors and to obtain precise information of the deuteron spin structure [13, 14]. The deuteron

 1310–0157

wave functions, which represent the basic ingredient in the investigation of elastic e-d scattering, can be computed with almost no approximations by using a realistic NN potential [15–18]. In addition to the deuteron wave functions, the nucleon structure is also an important ingredient in calculations of the elastic e-d scattering process. Theoretically, there exists a wide range of models and phenomenological parameterizations for nucleon form factors [6, 19–29]. Most of the theoretical models are based on effective meson theories, a few others on dispersion relations and the diquark model. The phenomenological parameterizations typically use polynomial functions, whose coefficients are fitted to the data. Modern semi-phenomenological models try to combine the meson-dominated low- and intermediate-energy region with the one governed by quark dynamics at higher energies.

The study of spin-dependent observables in elastic e-d scattering has the potential to enhance our understanding of internal nucleon and deuteron structure. It is well known that a wealth of detailed information is buried in polarization observables. This study is an important tool in order to investigate small, but interesting, dynamical effects, which normally are buried under the dominant amplitudes in unpolarized cross sections, but which often may show up significantly in certain polarization observables. A quite thorough discussion of polarization observables in elastic e-d scattering has been given in Refs. [4,6,9–11,29–37]. It was shown that the measurement of differential cross section and one polarization observable allows to extract the deuteron electromagnetic form factors. The influence of deuteron wave function from different NN potentials on polarization observables for elastic e-d scattering has been investigated and theoretical discrepancies among various models were found (see, for example, Ref. [12] and references therein). In addition, inconsistencies between the available data sets were obtained.

The main goal of the present work is to study the influence of different models of nucleon structure on the single tensor-deuteron and double beam-vector-deuteron analyzing powers in the elastic e-d scattering process. For the free-nucleon electromagnetic form factors, we use the standard dipole parameterizations (DFF) and the relativistic harmonic oscillator model (RHOM) given in Refs. [6, 29]. For the deuteron wave functions in the initial and final states, we use the realistic and high-precision CD-Bonn potential [38] which is the best version of all different versions of the Bonn potential. We give results for (i) the tensor-deuteron analyzing powers T_{20}, T_{21}, and T_{22} for polarized deuteron targets and unpolarized electron beams and (ii) the beam-vector-deuteron analyzing powers T_{10} and T_{11} for both polarized electron beams and polarized deuteron targets. We also compare our results for the elastic e-d scattering observables with the available experimental data from Refs. [1, 8, 39–44] in the case of T_{20}, T_{21}, and T_{22} and from Ref. [7] in the case of T_{10} and T_{11}. From this study we want to get information on a suitable description of the electromagnetic nucleon form factors, especially of the neutron electric form factor.

In Section 2, the fundamental ingredients of the elastic e-d scattering process are introduced. In Section 3, the relevant formalism for the cross section, structure functions, deuteron form factors, and analyzing powers for elastic e-d scattering are given. Section 4 will deal with the main results together with a comparison with the available experimental data. Finally, we summarize our results in Section 5.

2 Fundamental Ingredients

In this section, we briefly summarize the fundamental ingredients which are used in the present work to study the elastic e-d scattering process; the NN potential model adopted for the deuteron wave functions and the electromagnetic form factors of the nucleon.

During the past few decades, there are many realistic and high precision NN interaction models were developed (see Ref. [16] and references therein). These potentials are an important ingredient to the calculations of the few-body wave functions. In the present work, the deuteron wave functions in the initial and final states are taken from the realistic and high-precision CD-Bonn potential [38] which is the best version of all different versions of the Bonn potential. It is a charge-dependent one-boson-exchange NN potential that fits the world pp data below 350 MeV available in the year 2000 with a χ^2 per d.o.f. of 1.01 for 2932 data and the corresponding np data with χ^2/d.o.f. = 1.02 for 3058 data, where d.o.f. denotes degree of freedom. This reproduction of the NN data is more accurate than that by any phase-shift analysis and by any other NN potential. The charge dependence of the CD-Bonn potential is based upon the predictions by the Bonn potential (full model) for charge symmetry and charge-independence breaking in all partial waves with $J \leq 4$. The potential is represented in terms of the covariant Feynman amplitudes for one-boson exchange, which are nonlocal. Therefore, the off-shell behavior of the CD-Bonn potential differs in a characteristic way from commonly used local potentials and leads to smaller binding energies in nuclear few- and many-body systems.

For the electromagnetic form factors of the nucleon, there exist several models [6, 19–29]. For a long time the dipole fit for nucleon form factors was widely used [45]. Recently, there was an intensive discussion that the relation of proton electric form factor $G_E^p(Q^2)$ to the proton magnetic form factor $G_M^p(Q^2)$ obtained by the Rosenbluth separation technique [46] differs from the one obtained by the recoil polarization method [47, 48]. To describe the results of the latter method it is necessary to use a certain parameterization [47] for $G_E^p(Q^2)$. For the neutron electric form factor $G_E^n(Q^2)$ the Galster parameterization [23] can be used (see also Refs. [29] and [49]). In order to study the influence of nucleon structure on tensor-deuteron and beam-vector-deuteron analyzing powers, two different models from Refs. [6, 29] (see also Refs. [29, 45, 49–51]) are used

in the present work. We compare calculations with the standard dipole fit for the proton and neutron form factors with those where the relativistic harmonic oscillator model (RHOM) is used.

The standard dipole fit for the proton and neutron form factors (DFF) is given by

$$G_D(Q^2) = \left(1 + \frac{Q^2}{\Lambda^2}\right)^{-2}, \tag{1}$$

where $\Lambda^2 = 0.71$ (GeV/c)^2 and Q^2 is the four-momentum transfer squared. For the electric form factors of the proton and neutron, we, respectively, use

$$G_E^p(Q^2) = G_D(Q^2) \quad \text{and} \quad G_E^n(Q^2) = 0\,. \tag{2}$$

For the magnetic form factors of the proton and neutron, we use the following dipole parameterizations

$$G_M^p(Q^2) = \mu_p\, G_E^p(Q^2) \quad \text{and} \quad G_M^n(Q^2) = \mu_n\, G_E^p(Q^2)\,, \tag{3}$$

where $\mu_p = 2.7928$ and $\mu_n = -1.9130$ denote the magnetic moments (in nuclear magnetons) of the proton and neutron, respectively.

The relativistic harmonic oscillator model (RHOM) is based on the quark model with relativistic oscillator potential. All the form factors calculated in this model have the correct asymptotic behavior. The nucleon form factors are given using the function

$$I^{(3)}(Q^2) = \frac{1}{(1+2\tau_N)^2}\, \exp\left[\frac{-Q^2}{0.84(1+2\tau_N)}\right], \tag{4}$$

with $\tau_N = Q^2/(4M_N^2)$ is the Darwin-Foldy correction to the nucleon form factors, where M_N is the nucleon mass. The electric form factors of the proton and neutron are given, respectively, by

$$G_E^p(Q^2) = I^{(3)}(Q^2) \quad \text{and} \quad G_E^n(Q^2) = 2\tau_N\, I^{(3)}(Q^2)\,. \tag{5}$$

The magnetic form factors of the proton and neutron are given by

$$G_M^p(Q^2) = \mu_p\, I^{(3)}(Q^2) \quad \text{and} \quad G_M^n(Q^2) = \mu_n\, I^{(3)}(Q^2)\,. \tag{6}$$

3 Formalism for Elastic Electron-Deuteron Scattering

The differential cross section for the elastic scattering of unpolarized electrons of initial (final) energy E (E') from an unpolarized deuteron target with internal structure can be written in the Born approximation of a one-photon-exchange mechanism, neglecting the electron mass, as [52]

$$\frac{d\sigma_0}{d\Omega_e} = \left(\frac{d\sigma}{d\Omega}\right)_{Mott} \frac{E'}{E}\left[A(Q^2) + B(Q^2)\tan^2\frac{\theta_e}{2}\right], \tag{7}$$

where θ_e is the electron scattering angle in the laboratory frame and $Q^2 = 4EE' \sin^2(\theta_e/2)$. The Mott cross section is given by

$$\left(\frac{d\sigma}{d\Omega}\right)_{Mott} = \left[\frac{\alpha \cos(\theta_e/2)}{2E \sin^2(\theta_e/2)}\right]^2 , \tag{8}$$

with $\alpha = \frac{1}{137}$ is the fine-structure constant.

The unpolarized elastic structure functions $A(Q^2)$ and $B(Q^2)$ allow us to create a phenomenological description of the underlying structure of the deuteron. The structure function $A(Q^2)$ characterizes the charge distribution, whereas $B(Q^2)$ characterizes the distribution of the anomalous magnetic moment. These structure functions depend on the deuteron form factors and they are given in terms of the deuteron elastic form factors as [5]

$$A(Q^2) = \left[G_C^d(Q^2)\right]^2 + \frac{8}{9}\tau_d^2 \left[G_Q^d(Q^2)\right]^2 + \frac{2}{3}\tau_d \left[G_M^d(Q^2)\right]^2 , \tag{9}$$

$$B(Q^2) = \frac{4}{3}\tau_d(1+\tau_d) \left[G_M^d(Q^2)\right]^2 , \tag{10}$$

with $\tau_d = Q^2/(4M_D^2)$ denotes the Darwin-Foldy correction to the deuteron form factors, where M_D is the deuteron mass.

The charge, quadrupole, and magnetic deuteron form factors $G_C^d(Q^2)$, $G_Q^d(Q^2)$, and $G_M^d(Q^2)$, respectively, depend only on the radial deuteron wave functions and on the free nucleon form factors. These form factors can be written as [53,54]

$$G_C^d(Q^2) = G_E^S(Q^2)\, C_E^d(Q^2) , \tag{11}$$

$$G_Q^d(Q^2) = G_E^S(Q^2)\, C_Q^d(Q^2) , \tag{12}$$

$$G_M^d(Q^2) = 2G_M^S(Q^2)\, C_S^d(Q^2) + G_E^S(Q^2)\, C_L^d(Q^2) , \tag{13}$$

where $G_E^S(Q^2) = G_E^p(Q^2) + G_E^n(Q^2)$ and $G_M^S(Q^2) = G_M^p(Q^2) + G_M^n(Q^2)$ are the charge and the magnetic isoscalar nucleon form factors, respectively, and $G_{E,M}^{p,n}(Q^2)$ represent the electric and magnetic form factors of the proton and the neutron. The functions $C_E^d(Q^2)$, $C_Q^d(Q^2)$, $C_S^d(Q^2)$, and $C_L^d(Q^2)$, which describe the deuteron structure, involve overlaps of the deuteron wave functions $u(r)$ and $w(r)$, weighted by spherical Bessel functions. The nonrelativistic formulas for these form factors can be calculated from the deuteron $^3S_1$- and $^3D_1$-state wave functions, $u(r)$ and $w(r)$, respectively [55]

$$C_E^d(Q^2) = \int_0^\infty dr\; j_0\left(\frac{qr}{2}\right)\left[u^2(r) + w^2(r)\right] , \tag{14}$$

$$C_Q^d(Q^2) = \frac{3}{\sqrt{2}\tau_d}\int_0^\infty dr\; j_2\left(\frac{qr}{2}\right)\left[u(r) - \frac{w(r)}{\sqrt{8}}\right] w(r) , \tag{15}$$

$$C_S^d(Q^2) = \int_0^\infty dr \Big\{ \Big[u^2(r) - \frac{1}{2} w^2(r) \Big] j_0\Big(\frac{qr}{2}\Big) + \frac{1}{2} \Big[\sqrt{2} u(r) w(r) + w^2(r) \Big] j_2\Big(\frac{qr}{2}\Big) \Big\} , \tag{16}$$

$$C_L^d(Q^2) = \frac{3}{2} \int_0^\infty dr\, w^2(r) \Big[j_0\Big(\frac{qr}{2}\Big) + j_2\Big(\frac{qr}{2}\Big) \Big] , \tag{17}$$

where $j_0(x)$ and $j_2(x)$ are the spherical Bessel functions of order zero and two, respectively. The normalization condition is

$$\int_0^\infty dr\, [u^2(r) + w^2(r)] = 1 \, . \tag{18}$$

The standard deuteron form factors are normalized in the $Q^2 \to 0$ limit such that [5]

$$G_C^d(Q^2 \to 0) = 1 \, , \tag{19}$$

$$G_Q^d(Q^2 \to 0) = M_D^2 Q_D = 25.83 \, , \tag{20}$$

$$G_M^d(Q^2 \to 0) = (M_D/M_p)\mu_D = 1.714 \, , \tag{21}$$

where μ_D (in units of nuclear magnetons μ_N) and Q_D denote the static deuteron magnetic dipole and charge quadrupole moments, respectively, and M_D is the deuteron mass.

The differential cross section for elastic scattering of a longitudinally polarized electron beam from a polarized deuteron target is given in the laboratory frame by [56]

$$\begin{aligned} \frac{d\sigma}{d\Omega} = \left(\frac{d\sigma}{d\Omega} \right)_{Mott} & \left[1 + \frac{2E}{M_D} \sin^2 \frac{\theta_e}{2} \right]^{-1} \left[A(Q^2) + B(Q^2) \tan^2 \frac{\theta_e}{2} \right] \\ & \times \big[1 + \rho_{20} \cdot T_{20}(Q^2, \theta_e) + 2\Re e \rho_{21} \cdot T_{21}(Q^2, \theta_e) \\ & + 2\Re e \rho_{22} \cdot T_{22}(Q^2, \theta_e) + h \rho_{10} \cdot T_{10}(Q^2, \theta_e) \\ & + 2h \Re e \rho_{11} \cdot T_{11}(Q^2, \theta_e) \big] \, , \end{aligned} \tag{22}$$

where ρ_{kq} is a spherical tensor.

Defining $\mathcal{S}(Q^2, \theta_e) \equiv A(Q^2) + B(Q^2) \tan^2 \frac{\theta_e}{2}$, the tensor-deuteron T_{2M} $(M = 0, 1, 2)$ and the beam-vector-deuteron T_{1M} $(M = 1, 0)$ analyzing powers are given following to the Madison convention [57] in terms of the $G_C^d(Q^2)$, $G_Q^d(Q^2)$, and $G_M^d(Q^2)$ deuteron form factors as follows [5, 58]

(i) Tensor-deuteron analyzing powers:

$$\begin{aligned} T_{20}(Q^2, \theta_e) = -\sqrt{2} \, \frac{\tau_d}{\mathcal{S}(Q^2, \theta_e)} & \Big(\frac{4}{3} G_C^d(Q^2) G_Q^d(Q^2) \\ & + \frac{4}{9} \tau_d \left[G_Q^d(Q^2) \right]^2 + \frac{1}{6} \Big[1 + 2(\tau_d + 1) \tan^2 \Big(\frac{\theta_e}{2} \Big) \Big] \\ & \times \left[G_M^d(Q^2) \right]^2 \Big) \, , \end{aligned} \tag{23}$$

$$T_{21}(Q^2,\theta_e) = \frac{2}{\sqrt{3}}\,\frac{\tau_d}{\mathcal{S}(Q^2,\theta_e)}\,\sqrt{\tau_d+\tau_d^2\sin^2\left(\frac{\theta_e}{2}\right)} \times G_M^d(Q^2)\,G_Q^d(Q^2)\,\sec\left(\frac{\theta_e}{2}\right), \tag{24}$$

$$T_{22}(Q^2,\theta_e) = \frac{1}{2\sqrt{3}}\,\frac{\tau_d}{\mathcal{S}(Q^2,\theta_e)}\,\left[G_M^d(Q^2)\right]^2. \tag{25}$$

(ii) Beam-vector-deuteron analyzing powers:

$$T_{10}(Q^2,\theta_e) = \sqrt{\frac{2}{3}}\,\frac{\tau_d}{\mathcal{S}(Q^2,\theta_e)}\,\sqrt{(1+\tau_d)\left[1+\tau_d\sin^2\left(\frac{\theta_e}{2}\right)\right]} \times \left[G_M^d(Q^2)\right]^2\tan\left(\frac{\theta_e}{2}\right)\sec\left(\frac{\theta_e}{2}\right), \tag{26}$$

$$T_{11}(Q^2,\theta_e) = \frac{2}{\sqrt{3}}\,\frac{1}{\mathcal{S}(Q^2,\theta_e)}\,\sqrt{\tau_d(1+\tau_d)}\,G_M^d(Q^2) \times \left[G_C^d(Q^2)+\frac{\tau_d}{3}G_Q^d(Q^2)\right]\tan\frac{\theta_e}{2}. \tag{27}$$

4 Results and Discussion

In this section, we discuss the influence of the nucleon form factors on the results for the tensor-deuteron analyzing powers $T_{20}(Q^2,\theta_e)$, $T_{21}(Q^2,\theta_e)$, and $T_{22}(Q^2,\theta_e)$ for polarized deuteron targets and unpolarized electron beams as well as the beam-vector-deuteron analyzing powers $T_{10}(Q^2,\theta_e)$ and $T_{11}(Q^2,\theta_e)$ for both polarized electron beams and polarized deuteron targets in elastic e-d scattering. We present results for the various analyzing powers as functions of both Q^2 and θ_e. We also compare our predicted results for analyzing powers with the available experimental data.

The ingredients of the present work are the deuteron wave function and the free nucleon form factors. For the radial deuteron wave functions in the initial and final states, the realistic and high-precision CD-Bonn potential model [38] is used in the present work. For the free nucleon form factors, the standard dipole fit and the relativistic harmonic oscillator model [6, 29] are used to study the influence of nucleon structure on tensor-deuteron and beam-vector-deuteron analyzing powers.

Figure 1 shows the results for the tensor-deuteron analyzing power T_{20} as a function of Q^2 at various fixed values of θ_e (upper part) and as a function of θ_e at various fixed values of Q^2 (lower part). In order to study the dependence on nucleon form factors, results for the DFF and RHOM nucleon form factors are

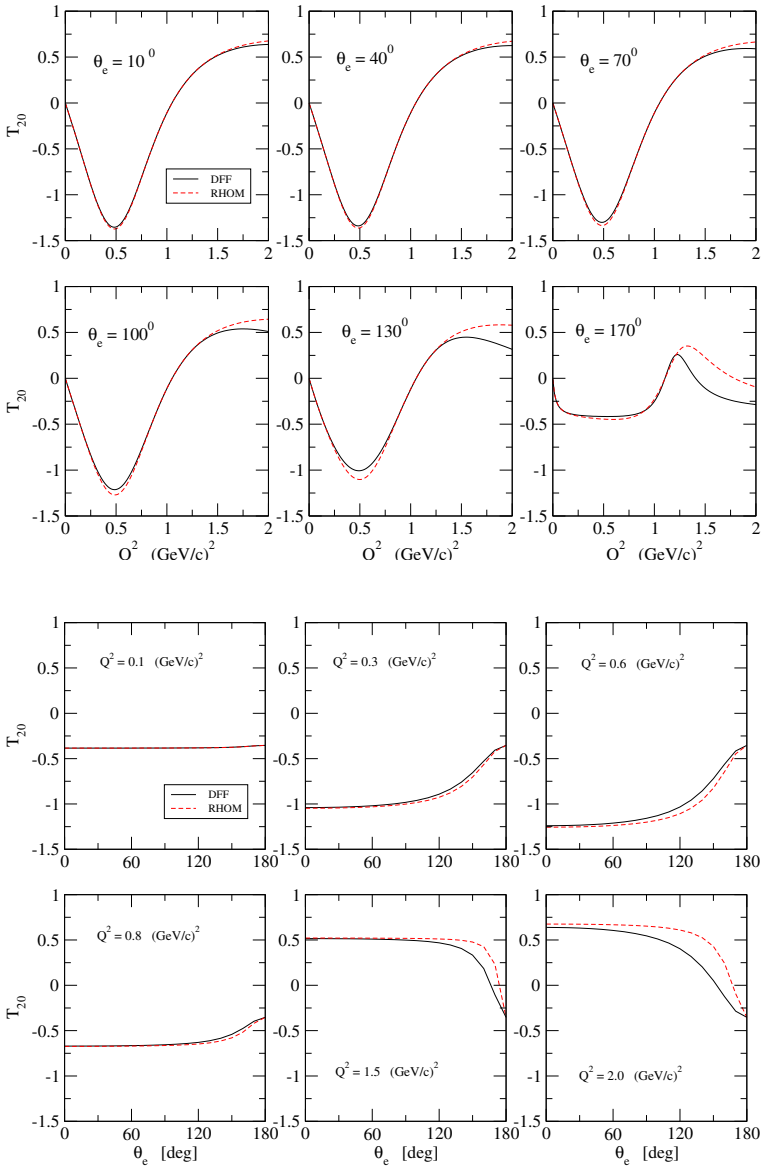

Figure 1. Influence of the tensor-deuteron analyzing power T_{20} as a function of Q^2 at various fixed values of θ_e (upper part) and as a function of θ_e at various fixed values of Q^2 (lower part) on nucleon form factors using the CD-Bonn potential [38] for the deuteron wave functions. The solid and dashed curves show the results for T_{20} using the DFF and RHOM nucleon form factors, respectively.

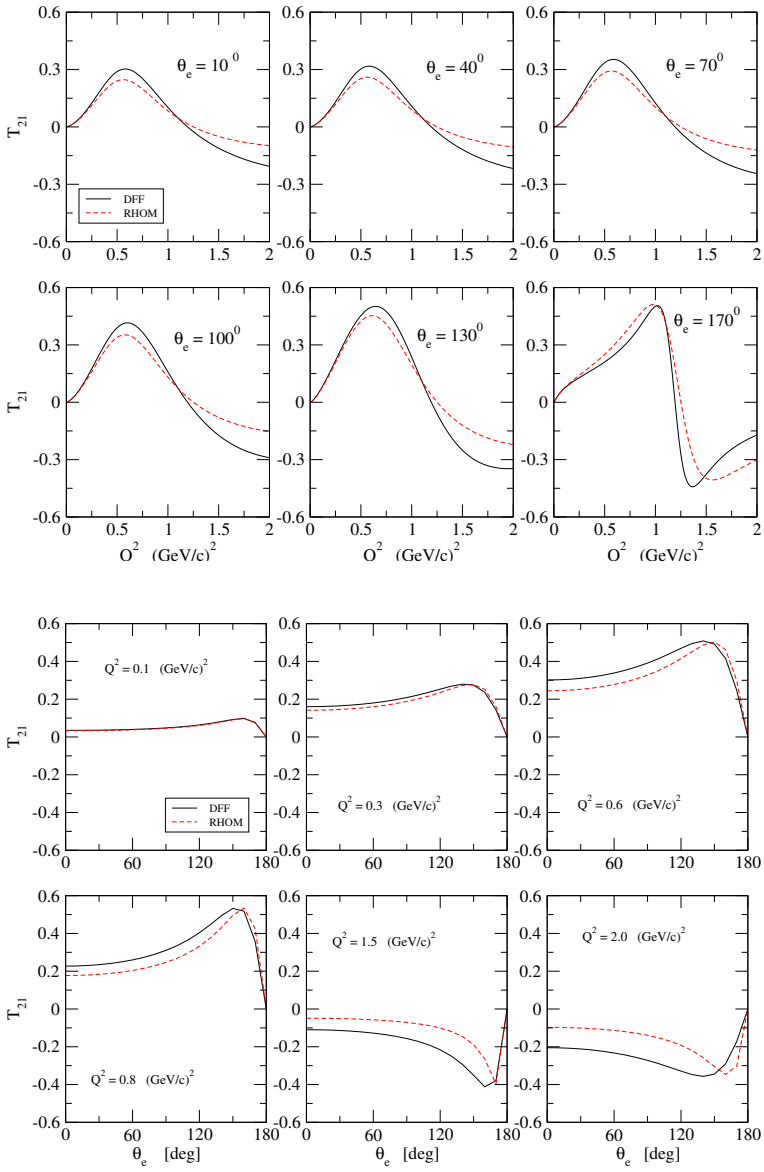

Figure 2. Same as in Figure 1 but for the tensor-deuteron analyzing power T_{21}.

given by the solid and dashed curves, respectively. We see from the upper part in Figure 1 that similar behaviors of the results for T_{20} up to $Q^2 \simeq 1.2$ (GeV/c)^2 and extreme backward direction are obtained when the DFF and RHOM models

are used. At higher values of Q^2, we see small differences between the results using various models for the nucleon form factors. The lower part in Figure 1 shows also that the T_{20} analyzing power is slightly influenced by the nucleon form factors. The difference between the solid (DFF) and dashed (RHOM) curves is almost negligible at forward direction and small Q^2 values. At extreme backward direction and $Q^2 > 1.2$ (GeV/c)^2, small differences between the results using DFF and RHOM models are observed. Figure 1 illustrates also that T_{20} slightly depends on the electron scattering angle. In addition, the T_{20} analyzing power is nearly independent on the nucleon form factors, in particular, on the poorly known neutron electric form factor.

In Figure 2 we present our results for the tensor-deuteron analyzing power T_{21} as a function of Q^2 at various fixed values of θ_e (upper part) and as a function of θ_e at various fixed values of Q^2 (lower part) using the DFF (solid curve) and RHOM (dashed curve) models for the nucleon form factors. It is also clear here that the results using the DFF and RHOM models for the nucleon form factors have the same behaviors. It is worth noticing that the T_{21} analyzing power is much more sensitive to the nucleon form factors than the T_{20} analyzing power. The upper part in Figure 2 displays that differences are found between the results for T_{21} using the DFF (solid curve) and RHOM (dashed curve) nucleon form factors at both forward and backward directions. The lower part in Figure 2 illustrates also that the T_{21} analyzing power is sensitive to the nucleon form factors since its results using the DFF and RHOM form factors are different. The difference between DFF and RHOM results increases with increasing Q^2 and θ_e. It is also obvious from Figure 2 that the T_{21} analyzing power vanishes at $\theta_e = 180^\circ$ and the difference between the solid and dashed curves reaches its maximum at $\theta_e = 0^\circ$.

The tensor-deuteron analyzing power T_{22} is plotted in Figure 3 as a function of Q^2 at various fixed values of θ_e (upper part) and as a function of θ_e at various fixed values of Q^2 (lower part) using the DFF (solid curve) and RHOM (dashed curve) models for the nucleon form factors. In contrast to T_{20} and T_{21}, the T_{22} analyzing power is seen to be small. One can see that the results of T_{22} using the DFF (solid curve) and RHOM (dashed curve) nucleon form factors have also similar behaviors. As in the case of T_{21} analyzing power, we found also here that T_{22} is sensitive to the nucleon form factors. We see from Figure 3 that the T_{22} analyzing power vanishes at $\theta_e = 180^\circ$ and the difference between the solid and dashed curves reaches its maximum at $\theta_e = 0^\circ$. The T_{21} and T_{22} analyzing powers are characterized by angular symmetry which is more pronounced for T_{22} at extreme backward direction.

Next, we present the results for the beam-vector-deuteron analyzing powers $T_{10}(Q^2, \theta_e)$ and $T_{11}(Q^2, \theta_e)$ for both polarized electron beams and polarized deuteron targets using various models for the nucleon form factors. These results are plotted in Figures 4 and 5. Figure 4 displays the influence of nucleon structure on the double beam-vector-deuteron analyzing power T_{10} as a function

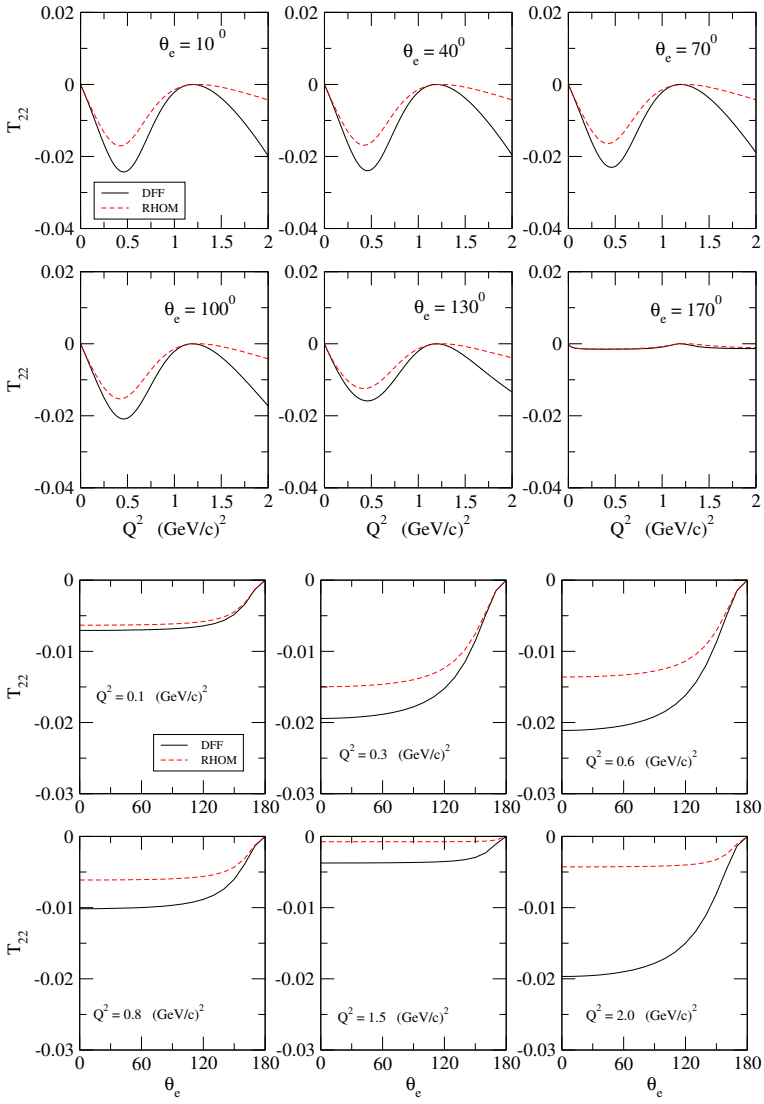

Figure 3. Same as in Figure 1 but for the tensor-deuteron analyzing power T_{22}.

of Q^2 at various fixed values of θ_e (upper part) and as a function of θ_e at various fixed values of Q^2 (lower part) using the DFF (solid curve) and RHOM (dashed curve) models for the nucleon form factors. As in the case of T_{20} analyzing power, we see that the influence of T_{10} on nucleon structure is negligible at extreme forward direction. At backward direction, a sizeable influence of nucleon structure on the results for T_{10} is obtained. The difference between the results

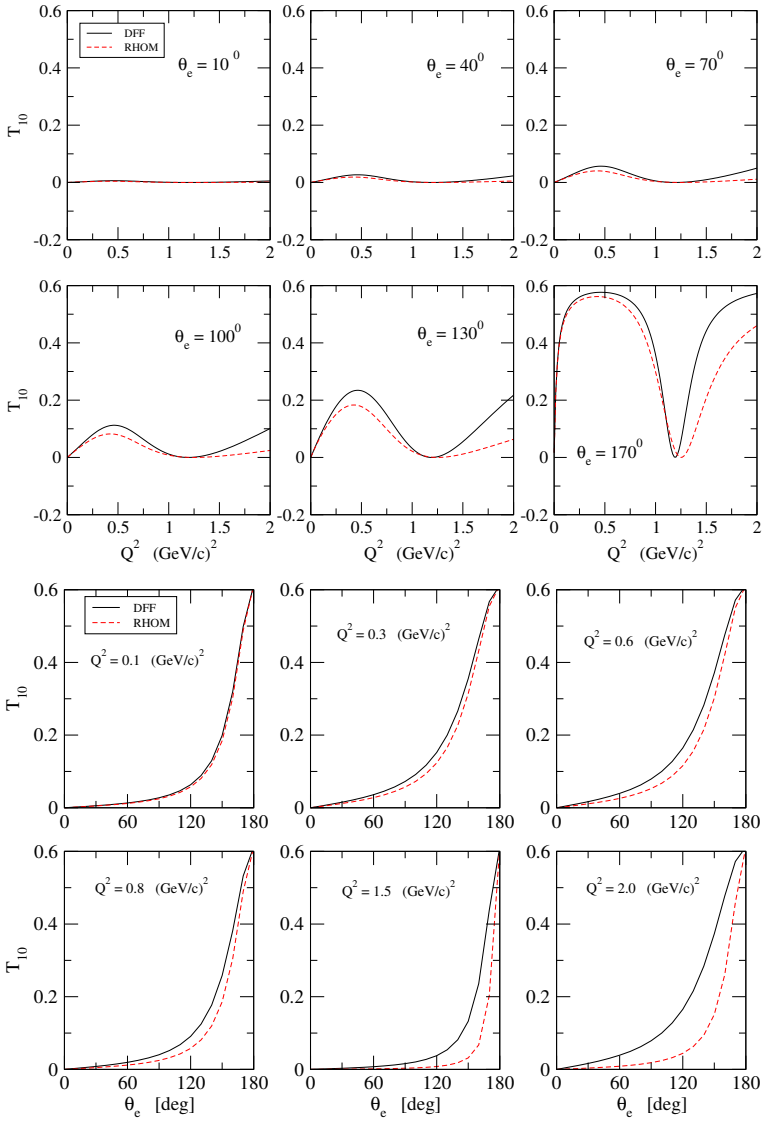

Figure 4. Same as in Figure 1 but for the beam-vector-deuteron analyzing power T_{10}.

using DFF (solid curve) and RHOM (dashed curve) form factors is large, specially at $Q^2 > 1.2$ (GeV/c)^2. It is also noticeable from Figure 4 that the T_{10} analyzing power vanishes at $\theta_e = 0°$ and increases with increasing θ_e until it reaches a maximum value at $\theta_e = 180°$.

The results for the beam-vector-deuteron analyzing powers $T_{11}(Q^2, \theta_e)$ are

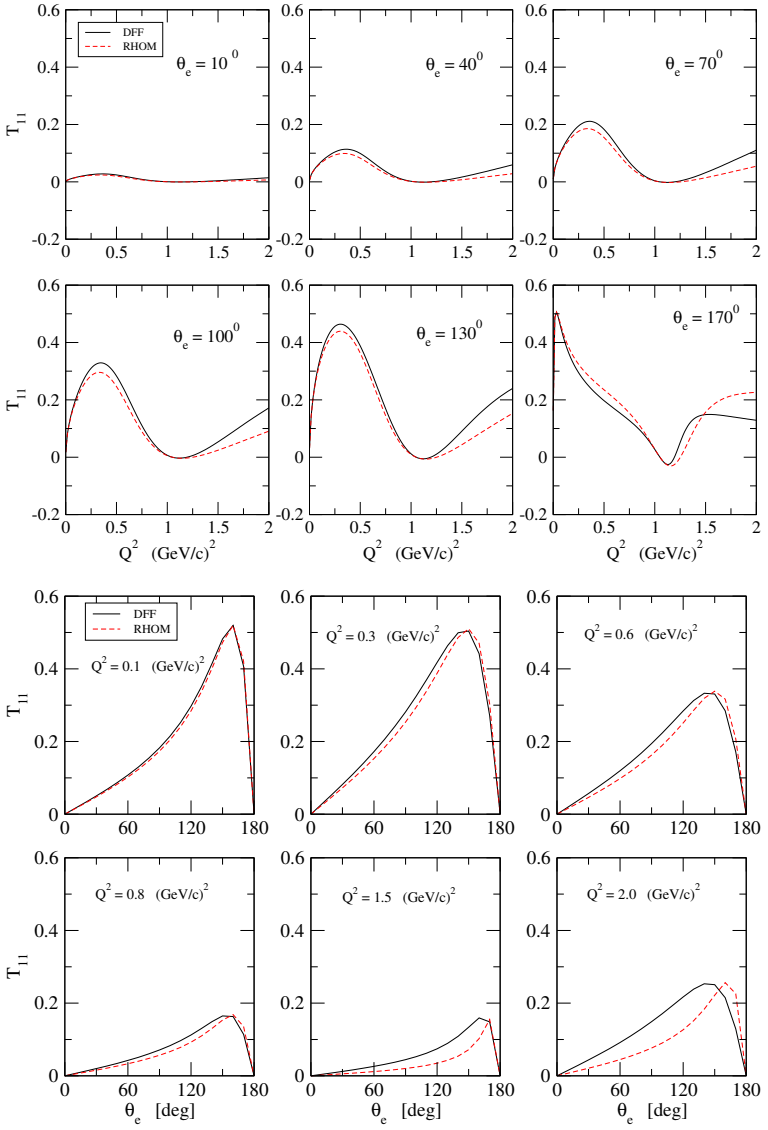

Figure 5. Same as in Figure 1 but for the beam-vector-deuteron analyzing power T_{11}.

shown in Figure 5 as a function of Q^2 at various fixed values of θ_e (upper part) and as a function of θ_e at various fixed values of Q^2 (lower part) using the DFF (solid curve) and RHOM (dashed curve) models for the nucleon form factors. As in the case of T_{10}, the influence on nucleon structure of the T_{11} analyzing power is almost negligible at forward direction. This influence is visible only at

backward direction and higher values of Q^2. Figure 5 shows also that the T_{11} analyzing power vanishes at $\theta_e = 0^\circ$ and 180°.

In contrast to the tensor-deuteron analyzing powers T_{20}, T_{21}, and T_{22}, the beam-vector-deuteron analyzing powers T_{10} and T_{22} are strongly dependent on the electron scattering angle θ_e. In addition, the T_{10} and T_{22} analyzing powers depend also on the choice of nucleon form factors. It is also obvious that the T_{10} analyzing power is smaller than T_{11} at the same electron scattering angle.

Now, we present a comparison between our results for various analyzing powers and the available experimental data as illustrated in Figure 6. The upper part display the tensor-deuteron analyzing powers $T_{2m}(Q^2, \theta_e = 70^\circ)$ $(m = 0, 1, 2)$ calculated with the deuteron wave functions from the CD-Bonn NN potential. Calculations with DFF (solid curve) and RHOM (dotted curve) nucleon form factors are shown in comparison to the experimental data are from MIT-Bates [1], MIT-Bates [8], MIT-Bates [39], Novosibirsk VEPP-2 [40], Novosibirsk VEPP-3 [41], NIKHEF [42], NIKHEF [43], and JLab [44]. In the lower part of Figure 6 we compare our results for vector-deuteron analyzing powers $T_{1m}(Q^2, \theta_e = 40^\circ)$ $(m = 0, 1)$ with the experimental data are from MIT-Bates [7].

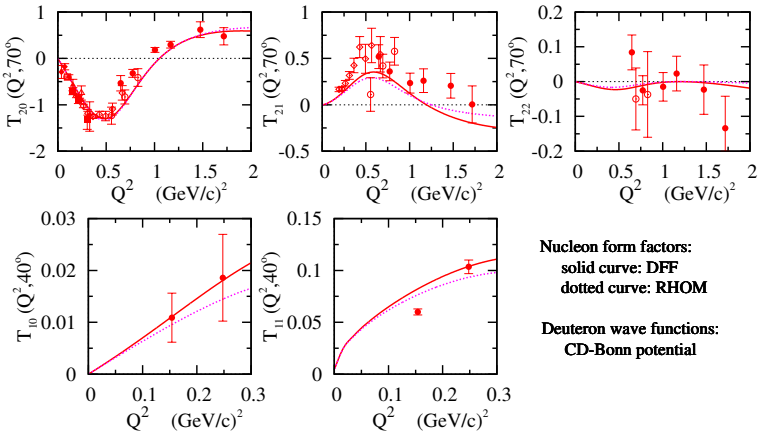

Figure 6. Upper panels: The tensor-deuteron analyzing powers $T_{2m}(Q^2, \theta_e = 70^\circ)$ $(m = 0, 1, 2)$ calculated with the deuteron wave functions from the CD-Bonn NN potential. Calculations with DFF (solid curve) and RHOM (dotted curve) nucleon form factors are shown. Experimental data are from MIT-Bates [1] (open circles), MIT-Bates [8] (open diamonds), MIT-Bates [39] (solid triangles), Novosibirsk VEPP-2 [40] (solid diamonds), Novosibirsk VEPP-3 [41] (open triangles), NIKHEF [42] (open squares), NIKHEF [43] (solid squares), and JLab [44] (solid circles). Lower panels: Same as in the upper panels but for vector-deuteron analyzing powers $T_{1m}(Q^2, \theta_e = 40^\circ)$ $(m = 0, 1)$. Experimental data are from MIT-Bates [7].

In general, one obtains a good agreement between our predictions for T_{20} and experimental data. In contrast to the T_{20} analyzing power, we see that the agreement between our predictions for T_{21} and the experimental data is unsatisfactory. One sees a satisfactory agreement only within the experimental errors. At $Q^2 > 0.6$ (GeV/c)^2, a better agreement between our calculations and the experimental data is obtained also within the error bars of the measurements. The measured $T_{21}(Q^2, \theta_e = 70^\circ)$ analyzing power has a maximum value higher than the theoretical maximum one. A possible source for the existing discrepancy between our predictions for T_{21} and the experimental data could be the neglected effects from meson-exchange currents, two (or more) photon exchange, isobar configuration in the deuteron wave function, and relativistic corrections. One might expect that the influence of these contributions maybe important for the theoretical description of observables for elastic e-d scattering. For example, the two-photon exchange mechanism was found to be important to extract the deuteron electromagnetic form factors from elastic e-d scattering [35]. Comparing our results for $T_{22}(Q^2, \theta_e = 70^\circ)$ analyzing power with the experimental data, we obtain a satisfactory agreement within the measurements errors. As for the doubly beam-vector-deuteron analyzing powers $T_{10}(Q^2, \theta_e = 40^\circ)$ and $T_{11}(Q^2, \theta_e = 40^\circ)$, a good agreement between our results and the experimental data from MIT-Bates [7] is obtained.

5 Summary

We have reported theoretical predictions for the tensor-deuteron analyzing powers T_{20}, T_{21}, and T_{22} and the beam-vector-deuteron analyzing powers T_{10} and T_{11} in the elastic electron-deuteron scattering process. The influence of the obtained results on the nucleon structure is investigated. In our calculations, we employed two models for the nucleon electromagnetic form factors which are the standard dipole parameterizations and the relativistic harmonic oscillator model given in Refs. [6, 29]. In addition, the results for analyzing powers are compared to the available experimental data from MIT-Bates [1, 8, 39], VEPP-2 [40], VEPP-3 [41], JLab [44], and NIKHEF [42, 43].

We found that the predicted results for the single tensor-deuteron analyzing powers T_{21} and T_{22} are sensitive to the nucleon form factors, specially at forward direction and $Q^2 > 1.2$ (GeV/c)^2. On the contrary, the T_{20} analyzing power is found to be independent on nucleon structure. As in the case of T_{21} and T_{22} asymmetries, we found that the predicted results for beam-vector-deuteron spin asymmetries T_{10} and T_{11} are influenced by the nucleon form factors when $Q^2 > 0.3$ (GeV/c)^2. Comparing the obtained results for single tensor-deuteron and double beam-vector-deuteron analyzing powers with the available experimental data, we see in general a satisfactory agreement within the experimental errors.

Future improvements of the present work can be achieved by including contributions from meson-exchange currents, two (or more) photon exchange, isobar configuration in the deuteron wave function, and relativistic (spin-orbit, Darwin-Foldy, and nuclear motion) corrections.

References

[1] M. Garçon *et al.* (1994) *Phys. Rev. C* **49** 2516; I. The *et al.* (1991) *Phys. Rev. Lett.* **67** 173; M. Garçon (1990) *Nucl. Phys. A* **508** 445c.

[2] J. Carlson and R. Schiavilla (1998) *Rev. Mod. Phys.* **70** 743.

[3] D. Abbott *et al.* (2000) *Eur. Phys. J. A* **7** 421.

[4] H. Arenhövel and S. K. Singh (2001) *Eur. Phys. J. A* **10** 183.

[5] M. Garcon and J. W. Van Orden (2001) *Adv. Nucl. Phys.* **26** 293.

[6] R. Gilman and F. Gross (2002) *J. Phys. G* **28** R37.

[7] P. J. Karpius (2005) *PhD dissertation, University of New Hampshire*.

[8] C. Zhang (2006) *PhD dissertation, MIT*.

[9] E. M. Darwish and M. Y. Hussein (2008) *J. Kor. Phys. Soc.* **52** 226.

[10] E. M. Darwish, M. Y. Hussein and B. Abu Sal (2009) *Appl. Math. & Inform. Sci.* **3** 309.

[11] E. M. Darwish, A. Abd El-Daiem and M. M. Abd El-Wahab (2017) *Phys. Part. Nucl. Lett.* **14** 822.

[12] E. M. Darwish, H. M. Abou-Elsebaa, E. M. Mahrous, and S. S. Al-Thoyaib (2019) *submitted for publication*; E. M. Darwish, E. M. Mahrous, and F. A. Alhazmi (2018) *AIP Conf. Proc.* **1976** 020008.

[13] E. M. Darwish (2015) *Incoherent Pion Photoproduction on the Deuteron: A Review* (LAMBERT Academic Publishing).

[14] E. M. Darwish and H. Mansour (2015) *π-Production off Deuteron Near η-Threshold: A Theoretical Overview* (LAMBERT Academic Publishing).

[15] R. Machleidt (2017) *Int. J. Mod. Phys. E* **26** 1730005.

[16] M. Naghdi (2014) *Phys. Part. Nucl.* **45** 924.

[17] J. Haidenbauer (2004) *Braz. J. Phys.* **34** 845.

[18] R. Machleidt and G.-Q. Li (1994) *Phys. Rept.* **242** 5.

[19] Y. Nambu (1957) *Phys. Rev.* **106** 1366.

[20] N. M. Kroll and T. D. Lee (1967) *Phys. Rev.* **157** 863.

[21] F. Iachello, A. D. Jackson and A. Lande' (1973) *Phys. Lett. B* **43** 191.

[22] E. Lomon (1980) *Ann. Phys. (N. Y.)* **1285** 309.

[23] S. Galster *et al.* (1971) *Nucl. Phys. B* **32** 221.

[24] M. Gari and W. Krümpelmann (1984) *Phys. Lett. B* **141** 295.

[25] M. Gari and W. Krümpelmann (1985) *Z. Phys. A* **322** 689.

[26] M. Gari and W. Krümpelmann (1986) *Phys. Lett. B* **173** 10.

[27] M. Gari and W. Krümpelmann (1992) *Phys. Lett. B* **274** 159.

[28] G. Höhler *et al.* (1976) *Nucl. Phys. B* **114** 505.

[29] K. S. Egiyan *et al.* (2007) *Phys. Rev. Lett.* **98** 262502; S. G. Bondarenko *et al.* (2011) *Few-Body Syst.* **49** 121; A. Bekzhanov *et al.* (2013) *Nucl. Phys. (Proc. Suppl.) B* **245** 65; A. Bekzhanov *et al.* (2014) *J. Exp. Theor. Phys. Lett.* **99** 613.

[30] M. Gourdin and C. A. Piketty (1964) *Nuovo Cimento* **32** 1173.

[31] D. Schildknecht (1964) *Phys. Lett.* **10** 254; D. Schildknecht (1965) *Z. Phys.* **185** 382.

[32] L. C. Alexa *et al.* (1999) *Phys. Rev. Lett.* **82** 1374.

[33] H. Arenhövel, F. Ritz and T. Wilbois (2000) *Phys. Rev. C* **61** 034002.

[34] A. F. Krutov and V. E. Troitsky (2007) *Phys. Rev. C* **75** 014001.

[35] G. I. Gakh and E. Tomasi-Gustafsson (2008) *Nucl. Phys. A* **799** 127.

[36] A. P. Kobushkin, Ya. D. Krivenko-Emetov and S. Dubnicka (2010) *Phys. Rev. C* **81** 054001.

[37] V. I. Zhaba (2017) *J. Phys. Stud.* **21** 4101.

[38] R. Machleidt, F. Sammarruca and Y. Song (1996) *Phys. Rev. C* **53** R1483; R. Machleidt (2001) *Phys. Rev. C* **63** 024001.

[39] M. E. Schulze *et al.* (1984) *Phys. Rev. Lett.* **52** 597.

[40] V. F. Dmitriev *et al.* (1985) *Phys. Lett. B* **157** 143.

[41] R. A. Gilman *et al.* (1990) *Phys. Rev. Lett.* **65** 1733.

[42] M. Ferro-Luzzi *et al.* (1996) *Phys. Rev. Lett.* **77** 2630.

[43] M. Bouwhuis *et al.* (1999) *Phys. Rev. Lett.* **82** 3755.

[44] D. Abbott *et al.* (2000) *Phys. Rev. Lett.* **84** 5053.

[45] H. Pietschmann and H. Stremnitzer (1969) *Lett. Nuovo Cim.* **2** 841.

[46] M. N. Rosenbluth (1950) *Phys. Rev.* **79** 615.

[47] O. Gayou *et al.* (2002) *Phys. Rev. Lett.* **88** 092301.

[48] M. K. Jones *et al.* (2000) *Phys. Rev. Lett.* **84** 1398.

[49] S. G. Bondarenko, V. V. Burov, and S. M. Dorkin (2000) *Phys. Atom. Nucl.* **63** 774 [(2000) *Yad. Fiz.* **63** 844]; S. G. Bondarenko, V. V. Burov and E. P. Rogochaya (2011) *Few Body Syst.* **49** 121.

[50] V. V. Burov *et al.* (1993) *Europhys. Lett.* **24** 443.

[51] C. Adamuscin *et al.* (2013) *Nucl. Phys. (Proc. Suppl.)* **245** 69.

[52] F. Gross (1966) *Phys. Rev.* **142** 1025; F. Gross (1966) *Phys. Rev.* **152** (E) 1517.

[53] M. I. Haftel, L. Mathelitsch and H. F. K. Zingl (1980) *Phys. Rev. C* **22** 1285.

[54] J. Arrington, C. D. Roberts and J. M. Zanotti (2007) *J. Phys. G* **34** S23.

[55] V. Jankus (1956) *Phys. Rev.* **102** 1586.

[56] T. W. Donnelly and A. S. Raskin (1986) *Ann. Phys. (N. Y.)* **169** 247.

[57] S. E. Darden (1971) in *Polarization phenomena in nuclear physics*, edited by H. H. Barschall and W. Haeberli (The University of Wisconsin Press, Madison, Wisconsin).

[58] R. G. Arnold, C. E. Carlson, and F. Gross (1981) *Phys. Rev. C* **23** 363.